Journal of Sound and Vibration (1997) **207**(3), 281–292

NUMERICAL ANALYSIS OF MEMBRANE STABILITY IN AIR FLOW

R. SYGULSKI

Institute of Structural Engineering, Poznań University of Technology, ul. Piotrowo 5, 60-965 *Poznań, Poland*

(*Received* 8 *February* 1994, *and in final form* 7 *November* 1995)

A numerical analysis of membrane stability in air flow is presented. The flow is treated as incompressible and potential. The divergent type and the flutter type of the loss of stability are studied. The problem is described by differential and integral equations, and the FEM and BEM are used to solve these equations, respectively. To discretize the membrane surface, triangular curvilinear six-node elements are applied. The eigenvalues of the matrix equation representing the quadratic eigenvalue problem give the complex frequencies of the membrane and enable one to predict whether the membrane motion is stable or unstable. Dimensionless stability analyses of circular, square and rectangular membranes are presented.

1. INTRODUCTION

In this paper, the stability analysis of a membrane in air flow is presented. The membrane is supported in an infinite baffle and coupled to an air half-space. Air flows over the membrane surface. The flow is treated as incompressible and potential. This model can be used as an approximation of more complex structures in an air flow. Membrane stability in an air flow has been considered in many papers [1–8]. This problem is well presented, especially in reference [1]. In most of these papers the flow is treated as two-dimensional and usually analytic methods are used in calculations.

Here a numerical approach to membrane stability in an air flow is presented. The numerical approach enables the stability analysis to be performed for any shape of the membrane, which is not possible with analytical methods. The membrane is discretized by elements that are simultaneously the finite elements for the membrane and the boundary elements for the air. Triangular curvilinear six-node elements are used. The velocity potential of the air satisfies the Laplace equation. The solution of this equation is expressed as a boundary integral equation. The boundary conditions on the surface are of the Neumann type. The problem is described by differential and integral equations. The finite element method (FEM) is used to solve the differential equations. Finite element equations are formulated by the weighted residuals method with Galerkin's criterion. The solution of the intergral equation is determined by means of the boundary element method (BEM). The eigenvalues of the matrix equation representing the quadratic eigenvalue problem give the complex frequencies of the structure and enable one to predict whether the structure motion is stable or unstable.

0022–460X/97/130281 + 12 $25.00/0/sv950790

2. PROBLEM FORMULATION

The membrane, of any shape, is supported in an infinite baffle (see Figure 1). The air flows over the membrane surface and does not flow under it. It is assumed that the air is incompressible and inviscid and the flow is potential and three-dimensional.

The perturbation air velocity potential $\varphi_1(\mathbf{x}, t)$ satisfies Laplace's equation

$$\nabla^2\varphi_1 = 0. \tag{1}$$

The integral solution of this equation for the half-space ($x_3 \geqslant 0$) has the form of a boundary integral equation. This is the Rayleigh integral equation [9] for the incompressible air:

$$\varphi_1(P, t) = \frac{1}{2\pi}\int_s \frac{\partial\varphi_1(Q, t)}{\partial x_3}\frac{1}{r(P, Q)}\,\mathrm{d}S_Q. \tag{2}$$

The boundary condition on the surface S is of the Neumann type and is the coupling conditions between the structure and the air. It is given by (see, e.g., reference [10])

$$\partial\varphi_1/\partial x_3 = \partial w/\partial t + U\partial w/\partial x_\alpha, \tag{3}$$

where $w = w(x_1, x_2, t)$ is the normal displacement of the membrane and U is the air flow velocity.

The perturbation pressure on the structure is (see, e.g., reference [10])

$$p_1 = -\rho(\partial\varphi_1/\partial t + U\partial\varphi_1/\partial x_\alpha), \tag{4}$$

where ρ is the air density. After the substitution $U = 0$ the perturbation pressure of the air under the membrane $p_2 = p_2(P, t)$ can be obtained by using equations (2)–(4). The resultant aerodynamic pressure is

$$p(P, t) = p_1(P, t) + p_2(P, t). \tag{5}$$

The linear equation of motion of the membrane is

$$T_1\partial^2 w/\partial x_1^2 + T_2\partial^2 w/\partial x_2^2 + \mu\partial^2 w/\partial t^2 = -p, \tag{6}$$

where μ is the mass of the membrane per unit area, and T_1 and T_2 are the membrane tensions per unit length in the x_1 and x_2 directions, respectively.

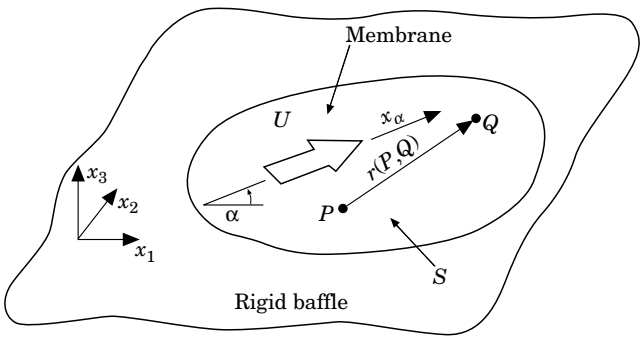

Figure 1. A membrane in flow.

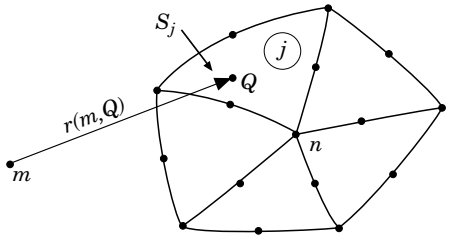

Figure 2. The notation for equation (16).

3. NUMERICAL SOLUTION OF THE PROBLEM

The pressure on the surface of the membrane is described by one boundary integral equation (2) and two differential equations (3) and (4). Upon separating the space and time variables and expressing the solution with respect to time in the exponential form (e.g., $p(P, t)=\tilde{p}(P)\,\mathrm{e}^{\lambda t}$, $\lambda=\gamma\pm\mathrm{i}\omega$, $\mathrm{i}=\sqrt{-1}$, ω is the circular frequency, γ is a coefficient influencing the amplitude (vibrations increase for $\gamma>0$)), equations (2)–(4) and (6) yield

$$\tilde{\varphi}_1(P)=\frac{1}{2\pi}\int_s \tilde{f}_1(Q)\,\frac{1}{r(P,Q)}\,\mathrm{d}S_Q, \qquad \tilde{f}_1=\lambda\tilde{w}+U\frac{\partial\tilde{w}}{\partial x_\alpha}, \tag{7, 8}$$

$$\tilde{p}_1=-\rho\left(\lambda\tilde{\varphi}_1+U\frac{\partial\tilde{\varphi}_1}{\partial x_\alpha}\right), \qquad -T_1\frac{\partial^2\tilde{w}}{\partial x_1^2}-T_2\frac{\partial^2\tilde{w}}{\partial x_2^2}+\lambda^2\mu\tilde{w}=\tilde{p}, \tag{9, 10}$$

where $\tilde{f}_1=\partial\tilde{\varphi}_1/\partial x_3$.

The finite element method is used to solve differential equations (8)–(10). The finite element equations are formulated by the method of weighted residuals with Galerkin's criterion [11]. The solution of the boundary integral equation (7) is determined by means of the boundary element method [12]. The surface of the structure is discretized by using six-node isoparametric curvilinear triangular elements. These elements are simultaneously the boundary elements for the air and the finite elements for the structure. Using the FEM to solve equations (8)–(10), one obtains the set of algebraic equations

$$\mathbf{B}_1\tilde{\mathbf{f}}_1=(\lambda\mathbf{B}_1+U\mathbf{B}_2)\tilde{\mathbf{w}}, \qquad \mathbf{B}_1\tilde{\mathbf{p}}_1=-\rho(\lambda\mathbf{B}_1+U\mathbf{B}_2)\tilde{\varphi}_1, \tag{11, 12}$$

$$(-\mathbf{T}_1\mathbf{B}_3-T_2\mathbf{B}_4+\lambda^2\mu\mathbf{B}_1)\tilde{\mathbf{w}}=\mathbf{B}_1\tilde{\mathbf{p}}, \tag{13}$$

where $\tilde{\mathbf{f}}_1$, $\tilde{\mathbf{w}}$, $\tilde{\mathbf{p}}$, $\tilde{\mathbf{p}}_1$, and $\tilde{\varphi}_1$ are the quantities in the element nodes forming the vectors. The matrices $\mathbf{B}_1$, $\mathbf{B}_2$, $\mathbf{B}_3$ and $\mathbf{B}_4$ are constructed from the finite element matrices $\mathbf{B}_1^e$, $\mathbf{B}_2^e$, $\mathbf{B}_3^e$ and $\mathbf{B}_4^e$, which are given by

$$\mathbf{B}_1^e=\int_{S_e}\mathbf{N}^{\mathrm{T}}\mathbf{N}\,\mathrm{d}S_e, \qquad \mathbf{B}_2^e=\int_{S_e}\mathbf{N}^{\mathrm{T}}\frac{\partial\mathbf{N}}{\partial x_\alpha}\,\mathrm{d}S_e,$$

$$\mathbf{B}_3^e=-\int_{S_e}\frac{\partial\mathbf{N}^{\mathrm{T}}}{\partial x_1}\frac{\partial\mathbf{N}}{\partial x_1}\,\mathrm{d}S_e, \qquad \mathbf{B}_4^e=-\int_{S_e}\frac{\partial\mathbf{N}^{\mathrm{T}}}{\partial x_2}\frac{\partial\mathbf{N}}{\partial x_2}\,\mathrm{d}S_e, \tag{14}$$

where $\mathbf{N} = [N_1, \ldots, N_6]$ is the matrix of element shape functions. The integrals (14) are computed numerically by using the Gauss integration formulas. The boundary element discretization of equation (7) results in the matrix equation

$$\tilde{\varphi}_1 = \mathbf{A}\tilde{\mathbf{f}}_1. \tag{15}$$

The elements A_{mn} of the matrix $\mathbf{A}$ are given by (see Figure 2)

$$A_{mn} = \frac{1}{2\pi} \sum_{j=1}^{e} \int_{S_j} N_n^{(j)} \frac{1}{r(m, Q)} \, \mathrm{d}S_Q, \tag{16}$$

where $N_n^{(j)}$ is the interpolation function for element j specified at the nth node and e denotes the number of elements coincident with node n. The integrals (16) are computed numerically by using the Gauss integration formulas. For $m = n$ a singularity of $1/r$ type occurs and special analytical–numerical integrations are adopted [13].

Using equations (15), (11) and (12) one obtains

$$\tilde{\mathbf{p}}_1 = -\rho[\lambda^2\mathbf{A} + \lambda U(\mathbf{A}\mathbf{B}_5 + \mathbf{B}_5\mathbf{A}) + U^2\mathbf{B}_5\mathbf{A}\mathbf{B}_5]\tilde{\mathbf{w}}, \tag{17}$$

where $\mathbf{B}_5 = \mathbf{B}_1^{-1}\mathbf{B}_2$. This equation represents the relationship between the vector of aerodynamic pressure amplitudes and the vector of displacement amplitudes of the membrane. After the substitution $U = 0$ in equation (17) one obtains the vector of pressure amplitudes for the air under the membrane:

$$\tilde{\mathbf{p}}_2 = -\rho\lambda^2\mathbf{A}\tilde{\mathbf{w}}. \tag{18}$$

Now substituting equations (17), (18) and (5) into the membrane equation (13) yields the homogeneous matrix equation

$$(\mathbf{K} + \lambda\mathbf{G} + \lambda^2\mathbf{M})\tilde{\mathbf{w}} = 0, \tag{19}$$

where $\mathbf{K} = \mathbf{K}_s + \mathbf{K}_a$, $\mathbf{M} = \mathbf{M}_s + \mathbf{M}_a$, $\mathbf{w} = \tilde{\mathbf{w}}\,\mathrm{e}^{\lambda t}$, $\lambda = \gamma \pm \mathrm{i}\omega$, $\mathrm{i} = \sqrt{-1}$, $\mathbf{K}_s = -T_1\mathbf{B}_3 - T_2\mathbf{B}_4$ is the stiffness matrix of the membrane, $\mathbf{M}_s = \mu\mathbf{B}_1$ is the mass matrix of the membrane, $\mathbf{M}_a = 2\rho\mathbf{B}_1\mathbf{A}$ is the fluid mass matrix, $\mathbf{K}_a = U^2\rho\mathbf{B}_1\mathbf{B}_5\mathbf{A}\mathbf{B}_5$ is the fluid stiffness matrix and $\mathbf{G} = U\rho\mathbf{B}_1(\mathbf{A}\mathbf{B}_5 + \mathbf{B}_5\mathbf{A})$ is the fluid gyroscopic matrix. Equation (19) is a quadratic

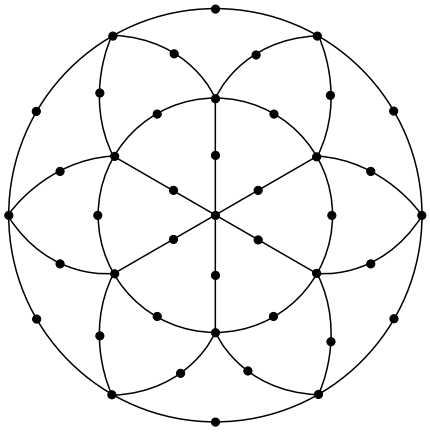

Figure 3. The discretization of a circular membrane.

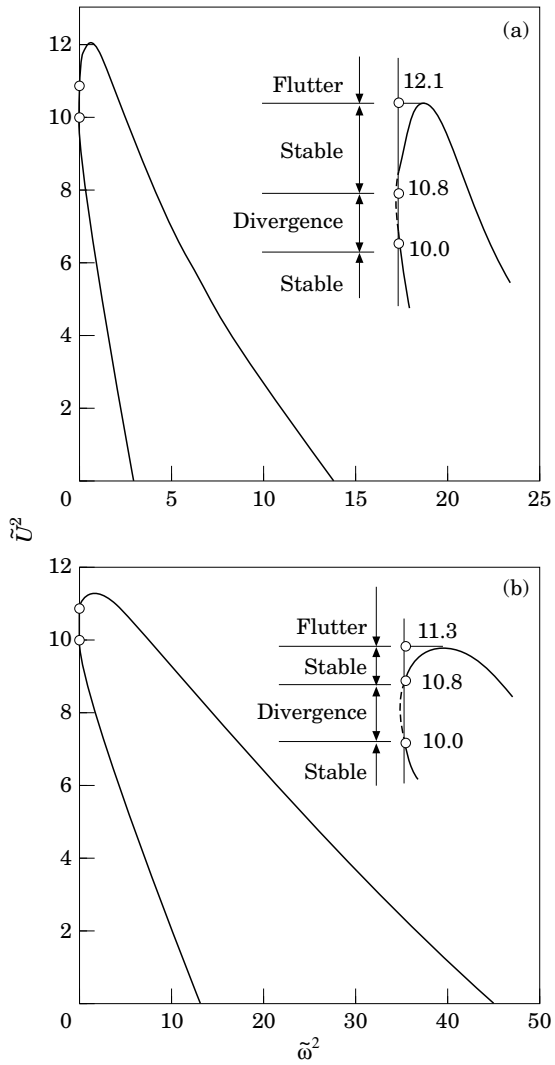

Figure 4. The $\tilde{U}^2$ versus $\tilde{\omega}^2$ diagram for a circular membrane, where $\tilde{U}$, $\tilde{\omega}$ and $\tilde{\mu}$ are the dimensionless flow velocity, frequency and mass of the membrane, respectively. (a) $\tilde{\mu} = 0{\cdot}1$; (b) $\tilde{\mu} = 1{\cdot}0$.

eigenvalue problem. By introducing the new variable $\mathbf{w}^* = \lambda\tilde{\mathbf{w}}$ it can be transformed to the standard eigenvalue problem

$$\begin{bmatrix} \mathbf{0} & \mathbf{I} \\ -\mathbf{M}^{-1}\mathbf{K} & -\mathbf{M}^{-1}\mathbf{G} \end{bmatrix} \begin{pmatrix} \tilde{\mathbf{w}} \\ \mathbf{w}^* \end{pmatrix} - \lambda \begin{pmatrix} \tilde{\mathbf{w}} \\ \mathbf{w}^* \end{pmatrix} = \begin{pmatrix} \mathbf{0} \\ \mathbf{0} \end{pmatrix}. \tag{20}$$

The eigenvalues of equation (20) for an assumed velocity flow U allow one to determine the character of the membrane motion and to predict whether the membrane motion is stable or unstable. For the case when $\lambda = 0$ (static loss of stability) equation (19) is reduced to

$$(\mathbf{K}_s - U^2\mathbf{K}_1)\tilde{\mathbf{w}} = \mathbf{0}, \tag{21}$$

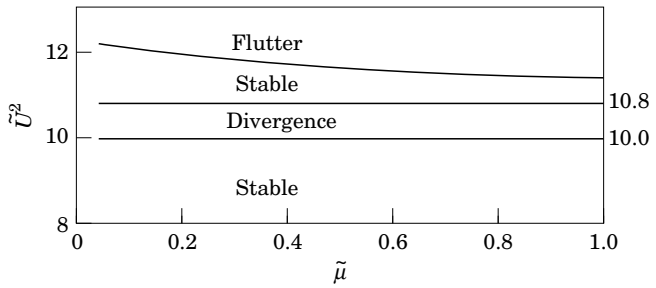

Figure 5. The various instability regions for a circular membrane in a $\tilde{U}^2$ versus $\tilde{\mu}$ diagram, where $\tilde{U}$ and $\tilde{\mu}$ are the dimensionless flow velocity and frequency.

where $\mathbf{K}_1 = -\rho\mathbf{B}_1\mathbf{B}_5\mathbf{A}\mathbf{B}_5$. Equation (21) is a generalized eigenvalue problem. By solving the problem one obtains the critical velocities of the divergent type instability of the membrane.

If the membrane is under flow with flow velocities U_1 above and U_2 below, then the fluid matrices $\mathbf{K}_a$ and $\mathbf{G}$ take the forms

$$\mathbf{K}_a = (U_1^2 + U_2^2)\rho\mathbf{B}_1\mathbf{B}_5\mathbf{A}\mathbf{B}_5, \qquad \mathbf{G} = (U_1 + U_2)\rho\mathbf{B}_1(\mathbf{A}\mathbf{B}_5 + \mathbf{B}_5\mathbf{A}). \tag{22}$$

If the damping forces are taken into acount in the membrane vibration analysis the membrane equation of motion (19) has the form

$$(\mathbf{K} + \lambda(\mathbf{C}_s + \mathbf{G}) + \lambda^2\mathbf{M})\tilde{\mathbf{w}} = \mathbf{0}, \tag{23}$$

where $\mathbf{C}_s$ is the damping matrix of the membrane (the other notation is as in equation (19)). A damping matrix proportional to the matrices $\mathbf{K}_s$ and $\mathbf{M}_s$ was adopted in the numerical analysis,

$$\mathbf{C}_s = \alpha\mathbf{K}_s + \beta\mathbf{M}_s, \tag{24}$$

where α and β are constant coefficients.

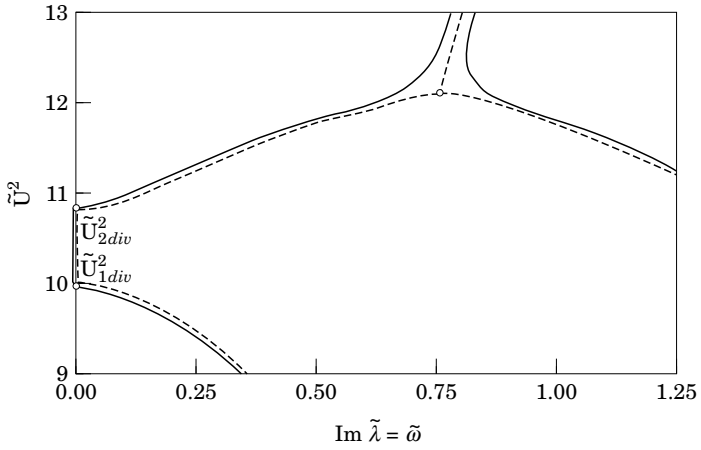

Figure 6. The $\tilde{U}^2$ versus Im $\tilde{\lambda}$ diagram for a circular membrane for the cases with (——) and without (– – –) damping.

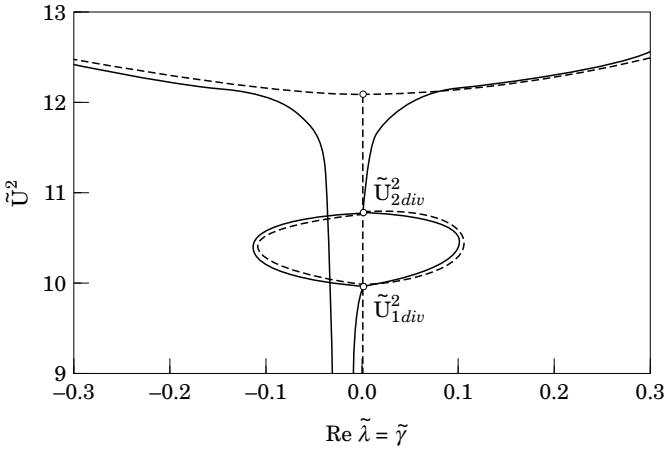

Figure 7. The $\tilde{U}^2$ versus Re $\tilde{\lambda}$ diagram for a circular membrane for the cases with (——) and without (– – –) damping.

4. NUMERICAL RESULTS

Based on problem formulation given in sections 2 and 3, computer programs were developed. The calculations were performed for three types of membranes: circular, square and rectangular.

4.1. EXAMPLE 1: THE CIRCULAR MEMBRANE

The membrane is discretized by 18 elements (Figure 3). The system has 31 degrees of freedom. The results of the dimensionless calculations are given in plots. The dimensionless parameters used in the analysis are defined as $\tilde{\omega}^2 = \omega^2 d^2 \mu / T$, $\tilde{U}^2 = U^2 \rho d / T$ and $\tilde{\mu} = \mu / \rho d$, where $\tilde{\omega}$ is the dimensionless frequency, $\tilde{U}$ is the dimensionless flow velocity, $\tilde{\mu}$ is the dimensionless mass of the membrane, T is the tension per unit width of membrane, μ is the mass of the membrane per unit area, d is the diameter of the membrane and ρ is the air density. The $\tilde{U}^2$ versus $\tilde{\omega}^2$ relationships for $\tilde{\mu} = 0{\cdot}1$ and $1{\cdot}0$ are given in Figures 4(a) and 4(b), respectively. Stable and unstable regions of membrane motion are marked in Figure 5. It can be observed from these figures that the first to occur is the divergent loss of stability. The region of divergence is narrow and does not depend on $\tilde{\mu}$. The membrane motion is then stable in the narrow region. That region is longer for smaller $\tilde{\mu}$. The increase

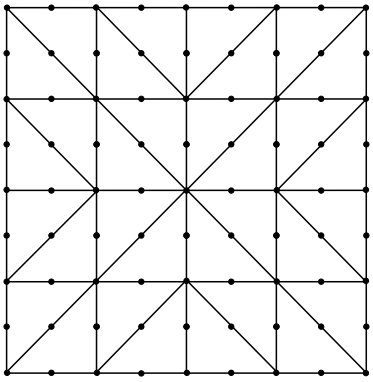

Figure 8. The discretization of a square membrane.

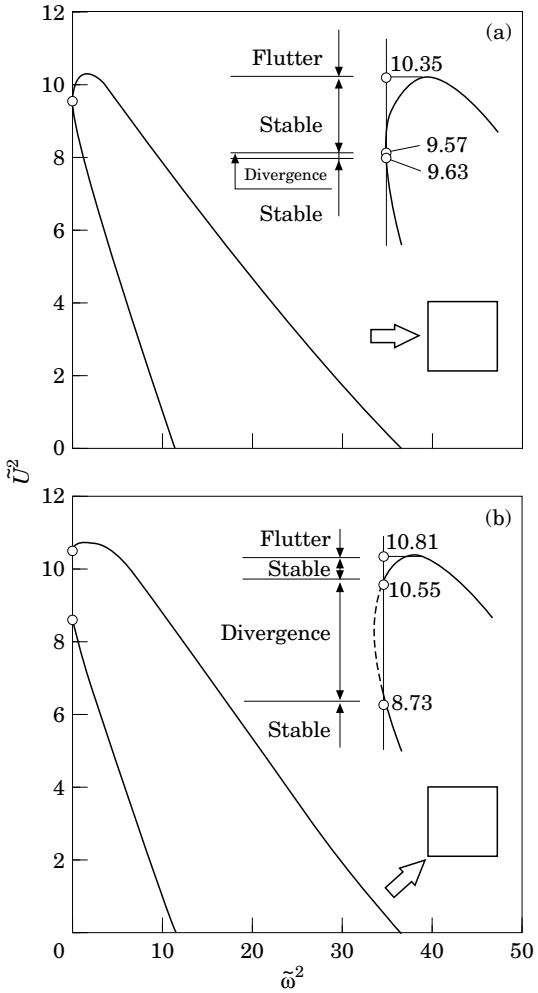

Figure 9. The $\tilde{U}^2$ versus $\tilde{\omega}^2$ diagram for a square membrane and for $\tilde{\mu} = 1{\cdot}0$, where $\tilde{U}$, $\tilde{\omega}$ and $\tilde{\mu}$ are the dimensionless flow velocity, frequency and mass of the membrane, respectively. (a) $\alpha = 0^\circ$; (b) $\alpha = 45^\circ$.

of velocity again causes the loss of stability, but of the flutter type. It is coupled mode flutter. It follows from Figure 4 that the structure under consideration, characterized by these eigenvalue curves, belongs to the so-called "hybrid type structure" classification (see reference [14]). The divergent loss of stability in subsonic flow occurs for simply supported plates and the cylindrical shells as well (see references [15, 17].

The analysis of the damping influence on the membrane stability shows that damping decreases the flutter velocity. In the case of the damped system the restabilization region vanishes and the flutter velocity is equal to the second divergence velocity ($U_{fl} = U_{2div}$). The results of calculations are presented in Figures 6 and 7. The $\tilde{U}^2$ versus Im $\tilde{\lambda}$ relationship for $\tilde{\mu} = 0{\cdot}1$, $\alpha = 0$ and $\tilde{\beta} = 0{\cdot}38$ is shown in Figure 6, and the U^2 versus Re $\tilde{\lambda}$ relationship is shown in Figure 7 ($\tilde{\lambda} = \lambda d\sqrt{\mu/T}$, $\tilde{\beta} = \beta d\sqrt{\mu/T}$, $\lambda = \gamma \pm \mathrm{i}\omega$). It is clear that for the damped membrane $\gamma > 0$ and $\omega \neq 0$ for $U > U_{2div}$; hence $U_{fl} = U_{2div}$.

4.2. EXAMPLE 2: THE SQUARE MEMBRANE

The membrane is discretized by 32 elements. The system has 49 degrees of freedom (see Figure 8). The results of dimensionless calculations are given in plots. The dimensionless

parameters used in the analysis are $\tilde{\omega}^2 = \omega^2 l^2 \mu / T$, $\tilde{U}^2 = U^2 \rho l / T$ and $\tilde{\mu} = \mu / \rho l$, where $\tilde{U}$ is the dimensionless flow velocity, $\tilde{\mu}$ is the dimensionless mass of the membrane and l is the span of the membrane. The other notations coincide with these from example 1. In Figures 9(a) and 9(b) are shown in the $\tilde{U}^2$ versus $\tilde{\omega}^2$ relationship for $\alpha = 0^\circ$ and 45°, respectively. For both cases, $\tilde{\mu} = 1$. Stable and unstable regions of membrane motion are marked in Figures 10(a) and 10(b) for $\alpha = 0^\circ$ and 45°, respectively. It can be observed from Figure 9(a) that the first and the second divergence velocities are nearly equal. The divergent instability region is very small.

4.3. EXAMPLE 3: THE RECTANGULAR MEMBRANE

The membrane is discretized by 32 elements, similarly to the square membrane. The results of the calculations for the first two divergence velocities for $\alpha = 0^\circ$, 45° and 90° and $b/l = 0{\cdot}8$ are presented in Table 1, where l is the membrane length, b is its width and the other notations are as for the square membrane. The modal shapes for the first divergence velocity for $\alpha = 0^\circ$, 45° and 90° and $b/l = 0{\cdot}8$ are given in Figures 11(a), 11(b) and 11(c),

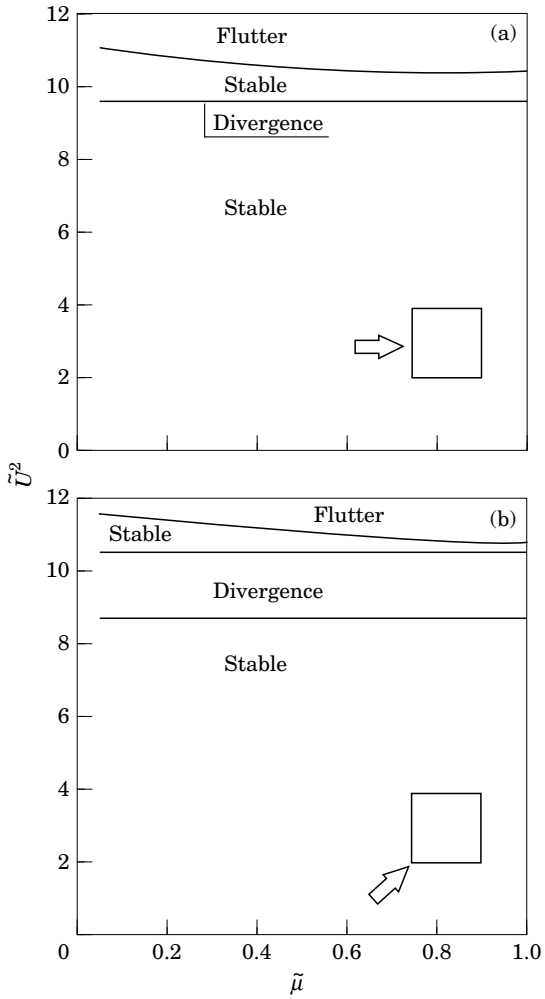

Figure 10. The various instability regions for a square membrane in a $\tilde{U}^2$ versus $\tilde{\mu}$ diagram, where $\tilde{U}$ and $\tilde{\mu}$ are the dimensionless flow velocity and mass of the membrane.

TABLE 1

The dimensionless divergence velocity for a rectangular membrane ($\tilde{U}^2 = U^2\rho l/T$, $b/l = 0{\cdot}8$)

Angle, α (degrees)	Dimensionless divergence velocity	
	$\tilde{U}_1$	$\tilde{U}_2$
0	3·331	3·483
45	3·152	3·437
90	3·104	3·304

respectively. One can see that the shape of the loss of stability for $\alpha = 0^\circ$ is similar to the second mode shape of the free vibration for the membrane.

Reference [6] gives the analytical solution for aeroelastic stability for the rectangular multi-span membranes. The divergence velocities for these membranes for $\alpha = 0^\circ$ are of the form

$$U^2_{n,m} = (\pi/\rho)\sqrt{(n/l)^2 + (m/b)^2}[T_1 + T_2(l/b)^2(m/n)^2] \tag{25}$$

and the modal shapes are

$$w(x_1, x_2) = a(n, m) \sin(n\pi x_1/l) \sin(m\pi x_2/b). \tag{26}$$

where $n, m = 1, 2, \ldots$, and l and b are the membrane dimensions in the x_1 and x_2 directions respectively. The dimensionless divergence velocities calculated from equation (25) for $T_1 = T_2 = T$ and $b/l = 0{\cdot}8$ are, for $\alpha = 0^\circ$, $\tilde{U}_{div} = 3{\cdot}210$, and for $\alpha = 90^\circ$, $\tilde{U}_{div} = 2{\cdot}872$. These values are a few percent smaller than those for the single membrane (see Table 1).

If $b \to \infty$ and $n = 1$, then equation (25) yields the solution for the 1-D multi-span membrane: $U^2_{div} = \pi T/\rho l$. Then the tension coefficient $C_T = T/(0{\cdot}5\rho U^2 l)$ is $C_T = (2/\pi) \simeq 0{\cdot}637$ for divergence. This result is equal to that given in reference [1].

5. CONCLUSIONS

A numerical method for study of the stability of membranes in incompressible and potential flow has been presented. The aerodynamic pressure associated with membrane deformations is described by boundary integral and differential equations. The finite element method for the membrane and the boundary element method discretization for the air are used. To discretize the surface of the membrane, triangular curvilinear six-node elements are applied. This formulation leads to non-symmetric and fully populated fluid matrices.

The numerical examples enable one to state the following main conclusions.

1. The divergence is responsible for the first loss of stability. The first divergence dimensionless velocity $\tilde{U}$ is about 3·16 for the circular membrane and about 3·10 and 2·95 for the square membrane for $\alpha = 0^\circ$ and 45°, respectively.

2.Coupled mode flutter occurs for $\tilde{U}$ greater then the second divergence velocity.

3. A small region of restabilization precedes the coupled mode flutter for the case of an undamped system. This region is longer for a small dimensionless mass of the membrane.

4. The membrane damping decreases the flutter velocity and the restabilization region is eliminated. The flutter velocity is then equal to the second divergence velocity.

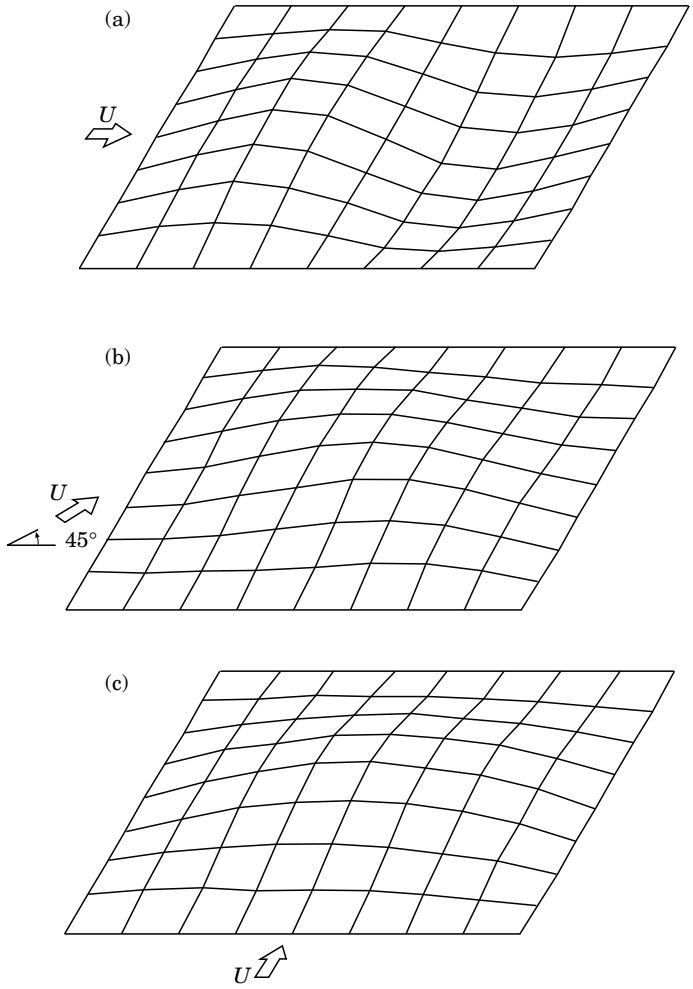

Figure 11. Modal shapes for the first divergence velocity for a rectangular membrane: (a) $\alpha = 0^\circ$; (b) $\alpha = 45^\circ$; (c) $\alpha = 90^\circ$ ($b/l = 0{\cdot}8$, where l and b are the membrane length and width).

ACKNOWLEDGMENT

Partial support by grant DS 11-016/95 is kindly acknowledged.

REFERENCES

1. B. G. Newman and M. P. Païdoussis 1991 *Journal of Fluids and Structures* **5,** 443–454. The stability of two-dimensional membranes in streaming flow.
2. B. G. Newman and M.-C. Tse 1980 *Journal of Fluid Mechanics* **100,** 673–689. Flow past a thin, inflated lenticular aerofoil.
3. B. G. Newman 1987 *Progress in Aerospace Science* **24,** 1–27. Aerodynamic theory for membranes and sails.
4. B. G. Newman and H. T. Low 1984 *Journal of Fluid Mechanics* **144,** 445–462. Two-dimensional impervious saills: experimental results compared with theory.
5. J. N. Nielsen 1963 *Journal of Applied Mechanics* **30,** 435–442. Theory of flexible aerodynamic surfaces.
6. R. Sygulski 1985 *Archiwum Inżynierii Lądowej* **31,** 471–482. Stability of multispan membrane covers subjected to the air stream (in Polish).

7. S. Kawamura and E. Kimoto 1971 *in Third International Conference on Wind Effects on Buildings and Structures*, *Tokyo*, *Japan*, 1067–1076. An aerodynamics stability of "oneway" types hanging roofs in the smooth, uniform flow.
8. H. Kunieda 1975 *International Journal of Solids and Structures* **11,** 477–492. Flutter of hanging roofs and curved membrane roofs.
9. Lord Rayleigh 1896 *Theory of Sound*. London: Macmillan.
10. R. L. Bisplinghoff and H. Ashley 1962 *Principles of Aeroelasticity*, New York: John Wiley.
11. K. H. Huebner 1975 *The Finite Element Method for Engineers*. New York: John Wiley.
12. C. A. Brebbia, J. C. F. Telles and L. C. Wrobel 1984 *Boundary Element Techniques*. Berlin: Springer-Verlag.
13. R. Sygulski 1993 *Computers and Structures* **49,** 867–876. Vibrations of pneumatic structures interacting with air.
14. H. Leipholz 1975 *Journal of the Engineering Mechanics Division*, **101,** 109–123. Aspects of dynamic stability of structures.
15. E. H. Dowell 1967 *Journal of the American Institute of Aeronautics and Astronautics* **5,** 1856–1862. Nonlinear oscillations of a fluttering plate, II.
16. C. H. Ellen 1973 *Journal of Applied Mechanics* **40,** 68–72. The stability of simply supported rectangular surfaces in uniform subsonic flow.
17. A. Kornecki 1974 *Journal of Sound and Vibration* **32,** 251–263. Static and dynamic instability of panels and cylindrical shells in subsonic potential flow.